ACS APPLIED MATERIALS & INTERFACES

Research Article

www.acsami.org

Superhydrophilic Polystyrene Nanofiber Materials Generating $O_2(^1\Delta_g)$: Postprocessing Surface Modifications toward Efficient Antibacterial Effect

Petr Henke,[†] Halyna Kozak,[‡] Anna Artemenko,[‡] Pavel Kubát,[§] Jitka Forstová,[†] and Jiří Mosinger*[,†,∥]

[†]Faculty of Sciences, Charles University in Prague, Hlavova 2030, 128 43 Prague 2, Czech Republic

[‡]Institute of Physics, v.v.i., Academy of Sciences of the Czech Republic, Cukrovarnická 10, 162 00 Prague 6, Czech Republic

[§]J. Heyrovský Institute of Physical Chemistry, v.v.i., Academy of Sciences of the Czech Republic, Dolejškova 3, 182 23 Prague 8, Czech Republic

[∥]Institute of Inorganic Chemistry, v.v.i., Academy of Sciences of the Czech Republic, 250 68 Řež, Czech Republic

Supporting Information

ABSTRACT: The surfaces of electrospun polystyrene (PS) nanofiber materials with encapsulated 1% w/w 5,10,15,20-tetraphenylporphyrin (TPP) photosensitizer were modified through sulfonation, radio frequency (RF) oxygen plasma treatment, and polydopamine coating. The nanofiber materials exhibited efficient photogeneration of singlet oxygen. The postprocessing modifications strongly increased the wettability of the pristine hydrophobic PS nanofibers without causing damage to the nanofibers, leakage of the photosensitizer, or any substantial change in the oxygen permeability of the inner bulk of the polymer nanofiber. The increase in the surface wettability yielded a significant increase in the photo-oxidation of external polar substrates and in the antibacterial activity of the nanofibers in aqueous surroundings. The results reveal the crucial role played by surface hydrophilicity/wettability in achieving the efficient photo-oxidation of a chemical substrate/biological target at the surface of a material generating $O_2(^1\Delta_g)$ with a short diffusion length.

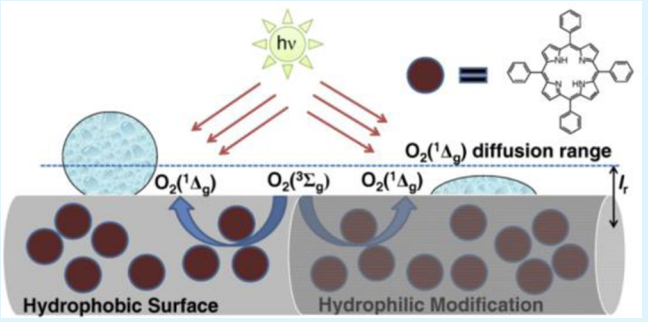

KEYWORDS: *nanofiber, singlet oxygen, photo-oxidation, antibacterial*

INTRODUCTION

The rapid development of novel nanomaterials based on polymer nanofibers for a broad range of applications such as filtration materials,[1] wound dressings,[2] scaffolds for tissue engineering,[3,4] and others has received great attention. The most common method of fabricating such nanofiber materials is via electrospinning from a polymer solution.[5] The electrospun materials, which have nanofiber diameters of approximately 100−400 nm, are characterized by a high surface area, transparency to light, high oxygen permeability/diffusion, and a nanoporous structure,[5,6] which prevent bacteria and other pathogens from passing through the nanofiber materials because they are detained on the surface.[7]

Recently, we have developed nanofiber materials with encapsulated porphyrinoid photosensitizers that generate $O_2(^1\Delta_g)$ at a high quantum yield upon irradiation with visible light. The small diameter of the nanofibers allows the efficient diffusion of $O_2(^1\Delta_g)$ outside the nanofibers and the photo-oxidation of chemical or biological targets. The short-living, highly cytotoxic $O_2(^1\Delta_g)$ efficiently kills bacteria such as *Escherichia coli, Staphylococcus aureus, Pseudomonas aeruginosa*,[8−11] nonenveloped polyomaviruses, and enveloped baculoviruses[12] on the surfaces of such nanofiber materials. Currently, these nanofiber materials are successfully applied in dermatology as antibacterial wound coverings that are activated by light.[11] A common feature of such polymeric nanofiber materials with encapsulated photoactive photosensitizers is a low diffusion length for $O_2(^1\Delta_g)$ (typically tens to hundreds of nanometers),[13] which limits the efficiency of the photo-oxidation of chemical/biological targets in proximity to the nanofiber surfaces. This problem is especially pertinent for the photo-oxidation of polar chemical/biological targets in aqueous solutions on the hydrophobic surfaces of polymer nanofiber materials, in which case the photo-oxidation is significantly decreased. More efficient photo-oxidation can be achieved by attaching a photosensitizer to the surfaces of the nanofibers[7] (where the photosensitizer is more sensitive and may possibly leak into the surroundings, thus limiting the applications of this approach) or near the surface, in which case the precise placement of the photosensitizer is difficult to control.[14]

Received: May 12, 2014
Accepted: July 11, 2014
Published: July 11, 2014

Another method of improving the photo-oxidation efficiency may involve increasing the surface wettability of the polymer nanofiber materials, which would increase the effective contact between the surface and the target.

The wettability of the surfaces of the polymers can be modified using various chemical and physical methods. In addition to traditional chemical-based surface modification, which consists of the introduction of polar groups on the polymer surfaces through a conventional reaction (e.g., through sulfonation), polymers of a highly hydrophilic nature are often achieved using oxygen plasma.[15−18]

The hydrophilicity/wettability of polymers treated with oxygen plasma is primarily attributed to the introduction of oxygen-containing functional groups on their surfaces. However, not all modifications can be attributed solely to the interaction of plasma radicals with the polymer. Oxygen plasma is a rich source of vacuum ultraviolet (VUV) radiation. This radiation is sufficiently energetic to break the bonds in polymers. The interaction of oxygen molecules with radicals that are created through the bombardment of the polymer with ions from the plasma can create hydroperoxides on the polymer surface. The instability of these hydroperoxides might contribute to the hydrophobic recovery that has been reported in some cases.[19] It has been observed that plasma treatment not only causes surface functionalization but also can change the surface morphology, especially in the 10 nm range.[20] Therefore, the hydrophilicity of the treated material depends on both the type and concentration of the surface oxygen functional groups as well as on the surface roughness.

Recently, it has been reported that catechols and compounds derived from them form self-assembled adhesive biocompatible coatings with increased wettability and cellular adhesion on various materials, including polymers.[21,22] In particular, dopamine, or 4-(2-aminoethyl)benzene-1,2-diol (DA), in the form of self-assembled polydopamine (PDA) has attracted considerable interest for biomedical applications varying from coatings for cell interfacing to drug delivery and biosensing.[21,22] The adhesiveness of PDA is attributable to amino, imino, hydroxyl, and catechol functional groups and $\pi-\pi$ interactions.[23] These functionalities cause PDA to be adhesive to all types of solid surfaces in aqueous or hydrated environments. PDA coating has been observed to exhibit antimicrobial activity against *E. coli*.[23] PDA that is formed through the oxidation of dopamine is composed of dihydroxyindole, indoledione, and dopamine units, which are assumed to be covalently linked; however, the detailed structure remains under investigation. In addition, an alternative structure has been proposed for PDA wherein the dihydroxyindole, indoledione, and dopamine units are not covalently linked to each other but instead are held together by hydrogen bonding or $\pi-\pi$ stacking.[24,25]

In the present work, we evaluate the role played by surface hydrophilicity/wettability in ensuring the efficient photo-oxidation of a chemical substrate/biological target in an aqueous environment at the surface of a material generating $O_2(^1\Delta_g)$ with a short diffusion length. We investigated the photophysical, photo-oxidative, and (photo)antibacterial properties of nanofiber materials with encapsulated hydrophobic 5,10,15,20-tetraphenylporphyrin photosensitizer (TPP) in hydrophobic polystyrene (PS) electrospun nanofibers before and after three simple postprocessing modifications: (i) sulfonation, (ii) cold oxygen plasma treatment, and (iii) PDA coating on the surface of the nanofiber material. Each modification can introduce interesting features into a pristine polymer matrix. In a previous study, we observed that after sulfonation, the PS nanofibers behaved as cationic ion exchangers, which can be used for the effective removal of heavy metals from an aqueous environment.[7] Cold oxygen plasma is a simple, widely used method for the introduction of oxygen-containing groups on the polymer surface, which can imbue the surface with antimicrobial properties.[26] In addition, PDA coating can endow the polymer matrix with new functions, such as UV shielding and radical scavenging.[27]

EXPERIMENTAL SECTION

Chemicals. 5,10,15,20-Tetraphenylporphyrin (TPP), cyclohexanone, tetraethylammonium bromide (TEAB), LB agar, LB medium, dopamine hydrochloride, tris(hydroxymethyl)aminomethane, KI, and other inorganic salts were purchased from Sigma-Aldrich and used as received. Sulfuric acid was used as received from Lach-Ner, Czech Republic. Polystyrene Synthos PS GP 137 was purchased from Synthos Kralupy a.s., Czech Republic. PBS was purchased from Lonza, Belgium.

Electrospinning. A mixture of 0.07 wt % TEAB and 99.93 wt % polystyrene (PS) was dissolved in cyclohexanone to prepare a 17% solution for the fabrication of the PS nanofiber material. Similarly, a mixture of 0.07 wt % TEAB, 98.93 wt % PS, and 1 wt % TPP in cyclohexanone was used for the fabrication of the PS nanofiber material with 1% TPP.

The nanofiber materials were produced using a modified Nanospider industrial electrospinning technology.[8] This device was used for the simultaneous formation of charged liquid jets on the surface of a thin wire electrode, where the number and location of the jets naturally assume their optimal positions (Figure S1, Supporting Information).[28] The diameters of the nanofibers were measured using the image analysis software NIS Elements 4.0 (Laboratory Imaging, Czech Republic). Before use, the pristine PS nanofiber material was thoroughly rinsed with deionized H_2O to remove trace TEAB.

Sulfonation. Electrospun PS nanofiber materials fixed on quartz substrates were treated by immersion in 96% sulfuric acid[29] at room temperature for 2 h. The materials were washed with deionized water and then neutralized with 25% ammonia hydroxide solution for approximately 24 h. Finally, the materials were washed with deionized water to achieve a neutral pH and stored in water.

Oxygen Plasma Treatment. PS nanofiber materials were oxidized in the radio frequency oxygen plasma using a low-pressure FEMTO plasma system (Diener Electronic GmbH & Co. KG) pumped down to a basic pressure of 8 Pa by scroll vacuum pump. The oxidation of nanofibers was provided in pure O_2 atmosphere at a pressure of 30 Pa with a power of 8 W during 20 s in order to ensure hydrophilic surface properties.

Polydopamine (PDA) Coating. Hydrophobic PS nanofiber materials were dipped in EtOH for 2 min to ensure good contact with the aqueous solution of dopamine. Then the materials were immersed in an aqueous solution of dopamine (2 mg/mL in 10 mM Tris, pH 8.5) for 30 min.[30] A light gray coating on the white surfaces of the PS materials, attributable to the self-polymerization of the dopamine, could be easily observed (Figure S2, Supporting Information).

Scanning Electron Microscopy (SEM). The nanofiber morphology was studied using a scanning electron Quanta 200 FEG microscope (FEI, Czech Republic).

Apparent Contact Angle Measurements. The hydrophobic/hydrophilic nature of the PS surfaces was characterized by performing apparent contact angle (ACA) measurements using a surface energy evaluation system (See System, Czech Republic). The ACAs of the PS surfaces before and after the modifications were measured using a 3 μL droplet of deionized water. Each measurement was repeated three times to obtain an average ACA value calculated through a multipoint fitting of the drop profile using the See System software. The same procedure was used to analyze the ageing of PS nanofibers in ambient

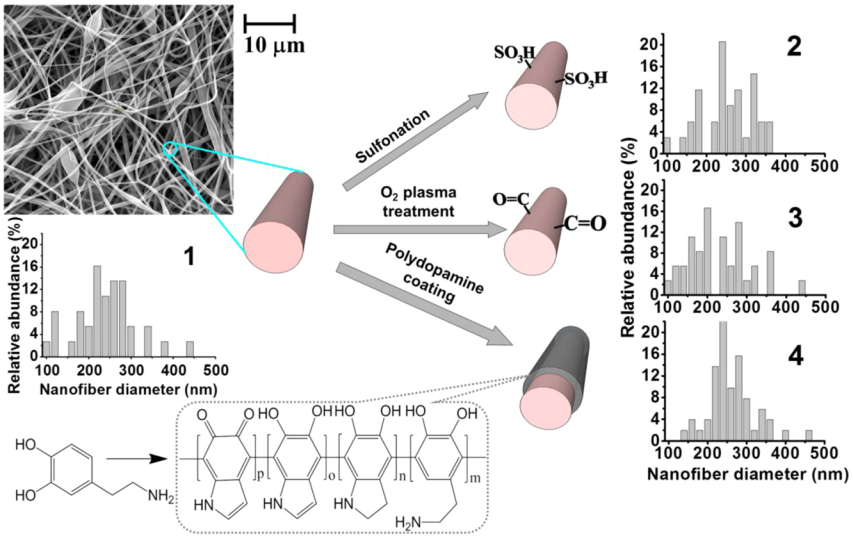

Figure 1. A scheme illustrating the preparation of samples **1**, **2**, **3** and **4** accompanied by the distributions of the nanofiber diameters, SEM image of sample **1** and reaction of the self-polymerization of dopamine.

air. The PS samples were stored in air at room temperature, in the dark, and with a constant relative humidity of ~22%.

Fourier Transform Infrared Spectra (FTIR). FTIR spectra were collected using a Thermo Nicolet 8700 FTIR spectrometer in the attenuated total reflectance (ATR) configuration using a Specac Gateway six-reflection horizontal ATR accessory with a ZnSe ATR prism. The ATR method was applied using an IR source, a KBr beam splitter, and a liquid-nitrogen-cooled photodiode (MCT) as a detector. The background spectrum was recorded using a clean ZnSe ATR prism without PS. During the measurements, the PS material was placed in an N_2-purged chamber of the FTIR spectrometer.

UV/Visible Absorption and Fluorescence Spectroscopy. The UV/vis absorption spectra were recorded using Unicam 340 and Cary 4000 spectrometers. The steady-state fluorescence spectra were monitored using an Aminco Bowman (AB2) spectrometer.

Time-Resolved Near-Infrared Phosphorescence of $O_2(^1\Delta_g)$. The time-resolved near-infrared phosphorescence of $O_2(^1\Delta_g)$ at 1270 nm was monitored using a Ge detector (Judson J16-8SP-R05M-HS) with excitation by a Lambda Physik Compex 102 excimer laser (λ_{exc} = 308 nm) or an F3002 dye laser (λ_{exc} = 425 nm). The short-lived signals produced by the scattering of the exciting laser pulse and by porphyrin fluorescence were eliminated by exciting the sample in vacuum and subtracting the obtained signal from the signal recorded in an oxygen or air atmosphere. Individual traces were accumulated 200–500 times to improve the signal-to-noise statistics.

Kinetics of Triplet States. Triplet states were recorded using an LKS 20 kinetic spectrometer (Applied Photophysics, U.K.). The samples were excited using the same lasers that were used for the phosphorescence measurements. The triplet states of TPP were monitored in both transmission and diffuse-reflectance modes. The kinetics of the triplet states of TPP were probed at 480 nm using a 250 W Xe lamp equipped with a pulse unit and an R928 photomultiplier.

Photo-Oxidation of Iodide Caused by Nanofiber Materials. A piece of the TPP-doped nanofiber material was placed in a thermostated 10 mm quartz cell (22 °C) that contained iodide detection solution. The cell was irradiated with visible light produced by a stabilized xenon lamp (500 W, Newport) with a long-pass filter ($\lambda \geq 400$ nm, Newport). The changes in the UV/vis absorbance at 351 nm, which were attributed to the formation of I_3^-, were recorded at regular intervals and compared with a blank solution of the same composition that was stored in the dark.[31]

Antibacterial Tests. A culture of *E. coli* K-12 was incubated under stirring in LB medium at 37 °C. Incubation was terminated when the absorbance at 560 nm reached a value of approximately 1. The prepared culture was diluted 2000× to the desired concentration in PBS. The nanofiber materials (5 cm^2) with or without encapsulated TPP were placed on bacterial agar plates. The surfaces of the materials were inoculated with 3 × 20 μL (approximately 6000 colony-forming units (CFUs)) of a suspension of *Escherichia coli* in PBS. The agar plates either were illuminated with white light from a 400 W solar daylight simulator (Sol1A Newport, USA) with a water filter (for elimination of the heating effect) for 5, 10, 15, or 20 min or were stored in the dark. Then the samples were placed in Eppendorf tubes with 1 mL of PBS. After brief shaking (2× 3 s on an IKA vortex 3), the PS nanofiber matrix was removed. Each bacterial suspension was centrifuged for 5 min at 3600*g* (7000 rpm). The supernatant (0.7 mL) was carefully removed. From the pellet media, 100 μL of each bacterial suspension was placed on sterile agar plates. The plates were incubated for 15 h in darkness at 37 °C to allow the individual bacteria to grow and form colonies.

RESULTS AND DISCUSSION

Preparation of Nanofiber Materials. The preparation of the nanofiber materials with TPP encapsulated in PS electrospun nanofibers before and after the postprocessing modifications via sulfonation, oxygen plasma treatment, and polydopamine (PDA) coating is described in the Experimental Section and schematically described in Figure 1. The resulting material consisted of some irregularities, such as nodes and bundles of nanofibers.

The structure of the electrospun polystyrene (PS) nanofiber materials (**1**) was visualized through scanning electron microscopy (SEM). Figure 1 and Figure S2 (Supporting Information) present SEM images of the nanofiber materials before (**1**) and after postprocessing modifications through sulfonation (**2**), oxygen plasma treatment (**3**), and PDA coating (**4**). The nanofiber structure of the materials remained intact after 2 h of sulfonation in concentrated H_2SO_4, 20 s of oxygen plasma treatment, or 30 min of incubation in PDA solution (see Experimental Section). The average diameters of the nanofibers before the postprocessing modifications (**1**, 248 ± 29 nm) and after sulfonation (**2**, 253 ± 22 nm), oxygen plasma treatment (**3**, 232 ± 20 nm), and PDA coating (**4**, 268 ± 21 nm) remain almost unchanged.

ATR-FTIR Spectra. To verify the chemical changes in the PS nanofibers before and after treatment, FT-IR signals were recorded (Figure 2). The FTIR spectrum of the original PS

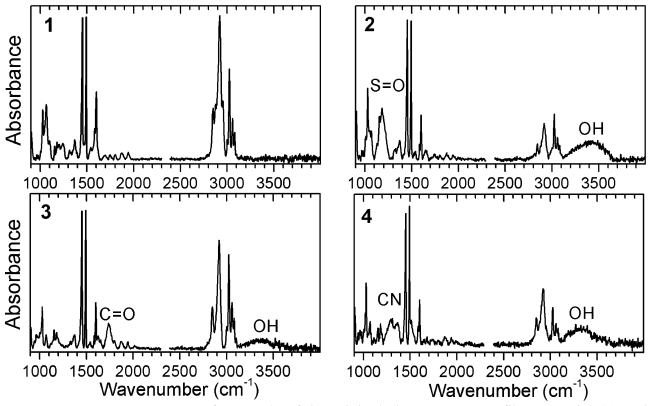

Figure 2. ATR-FTIR spectra of a sample of the original electrospun nanofiber material (**1**) and the corresponding samples after surface modifications (**2**, **3**, and **4**).

nanofiber material **1** reveals the presence of typical PS functional groups: bands corresponding to aromatic C−H stretching modes between 2850 and 3080 cm^{-1}, an overtone and combination band associated with C−H out-of-plane bending at 1660−2000 cm^{-1}, C−C stretching vibrations at 1600 cm^{-1}, C−H aromatic-ring vibrations at 1491 cm^{-1}, C═C aromatic-ring vibrations at 1450 cm^{-1}, bands associated with aromatic-ring C−C stretching and aromatic C−H in-plane bending at 1000−1200 cm^{-1}, and bands near 965 and 910 cm^{-1} associated with CH out-of-plane vibrations.[32] In the spectrum of **2**, the region between 1300 and 900 cm^{-1} clearly reveals changes associated with the sulfonate stretching bands. The intensity of the doublet bands at 1180 and 1155 cm^{-1}, which correspond to asymmetric and symmetric S═O stretching vibrations, respectively, strongly increased. The spectra of **2** and **4** reflect a decrease in the intensity of the CH bands at 2850−3080 cm^{-1} and an increase in the intensity of the OH-related band compared with the original PS materials.

The spectrum of **3** indicates that the oxygen plasma treatment introduced a new band at 1743 cm^{-1}, which is assigned to the stretching of carbonyl C═O groups. The spectrum also indicates the presence of a very broad band at 3100−3500 cm^{-1}, which most likely corresponds to hydroxyl groups from the oxygen species and/or adsorbed water.

In the spectrum of **4**, the broad band at 3100−3400 cm^{-1} can be assigned to the hydroxyl stretching vibrations of the adsorbed water that overlap the stretching vibrations of the amino groups (NH_2). The new peak at 1300 cm^{-1} most likely corresponds to C−N stretching vibrations.

Apparent Contact Angle Measurements. This method is commonly used for differentiation between hydrophobic and hydrophilic nature of nanofiber samples.[33,34] It provides only qualitative information and can be used only for comparison of samples with the same or similar structure.

The original electrospun PS nanofiber material (**1**) washed with deionized H_2O to remove trace of TEAB additive exhibited hydrophobic properties with an apparent contact angle (ACA) of approximately 130 ± 4°. The traces of polar TEAB can alter the surface properties of nanofibers. All surface modifications dramatically changed this hydrophobic PS surface into highly hydrophilic surfaces with ACAs below 5° (Figure 3 and Figure S5 in Supporting Information). The low value of ACAs may be also influenced by the tendency of water droplets to immerse through pores. This effect allows diffusion of photoxidation targets into porous structure of the materials,

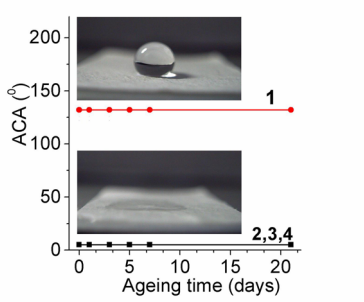

Figure 3. ACA measurements of samples **1** (red, 130°), **2**, **3**, and **4** (black, <5°) in time. Upper picture shows water droplet on the surface of sample **1**. Lower picture shows the same on the surface of sample **3**.

where they can be attacked easily by $O_2(^1\Delta_g)$ than on the surface of the materials.

The observed ACA for the original PS nanofiber material was smaller than that reported in the literature (155 ± 3°),[33] most likely because of the greater roughness of the surface. In addition, for the PDA coating, the observed ACA was not consistent with the published values of 50−60° that have been observed for this coating applied to other materials.[35] Evidently, the nanoporous nature of the materials employed in this study strongly affected the ACA, with a tendency toward higher wettability. It is also known that in some cases, the functionalization of a polymer through the nonequilibrium oxygen plasma treatment of the samples can cause either the decay or reorientation of the functional groups on the surface. These effects can lead to a loss of surface wettability.[19,20] However, a change in the surface wettability can also be ascribed to many other effects, such as those to surface charge and roughness as well as changes in the chemical structure of the material.[36] The water-drop ACAs of all samples were determined after various storage times. The same ACAs of all samples were observed during their ageing in open air after the same elapsed times (Figure 3, red and black curves). The ACAs of the nanofiber materials (**1**, **2**, **3**, and **4**) were identical to those of the materials with encapsulated TPP photosensitizer (**1-TPP**, **2-TPP**, **3-TPP**, and **4-TPP**).

An interesting phenomenon was observed for the PS nanofiber material with PDA coating on only one side, e.g., after treatment of the material coiled on quartz surface. For some experiments, the solid support may be removed. The resulting Janus nanofiber material exhibited properties similar to those of a nanofiber material based on the polyamide matrix.[34] On the untreated side, the PS material exhibited hydrophobic properties, with a water contact angle of 130 ± 4°, whereas the opposite side of the material was converted into a highly hydrophilic surface (ACA less than 5°). When this material was placed on a water surface, the effects of self-orientation and self-stretching were observed, most likely because of the combination of the hydrophobic effect of the untreated side and the effect of hydrogen bonding on the side with the PDA coating (Figures S3 and S4, Supporting Information).

UV/Visible Absorption and Fluorescence Spectra. UV/vis absorption and fluorescence spectra were measured to evaluate the effects of the postprocessing modifications of the materials on the encapsulated TPP. The untreated, TPP-doped PS nanofiber material (**1-TPP**) exhibited characteristic porphyrin absorption and fluorescence spectra: a Soret band at 421 nm, four Q bands at 516, 550, 592, and 648 nm, and

fluorescence emission bands at 653 and 719 nm. These values are similar to those of TPP in organic solvents, e.g., CH_2Cl_2. The absorption and emission spectra of the photosensitizer encapsulated in the PS nanofibers before (**1-TPP**) and after postprocessing modifications (**2-TPP**, **3-TPP**, and **4-TPP**) were essentially identical (Figures S6, S7, and S8, Supporting Information). The formation of porphyrin dimers and higher aggregates, which is typically accompanied by red or blue shifts and broadening of the Soret band[37,38] or quenching of the fluorescence, was not observed. The observations indicated that the 1 wt % TPP that was incorporated into the PS nanofibers remained predominantly in the monomeric state even after the surface modifications.

Kinetics of the Triplet State and Singlet Oxygen $O_2(^1\Delta_g)$. In our previous study, we presented the kinetics of ^{3}TPP encapsulated in unmodified PS nanofibers and the photogeneration of $O_2(^1\Delta_g)$ using time-resolved spectroscopy.[13] The kinetics of ^{3}TPP can be described as follows:

$$[^3\mathrm{TPP}] = [^3\mathrm{TPP}_0] \exp(-t/\tau_T) \quad (1)$$

$$1/\tau_T = 1/\tau_{T0} + k_q p_{O2} \quad (2)$$

where τ_{T0} and τ_T are the lifetimes of ^{3}TPP in vacuum and in an oxygen atmosphere, respectively, p_{O2} is the oxygen pressure, and k_q is the bimolecular constant of the quenching of ^{3}TPP by oxygen.

The singlet oxygen was directly measured from the phosphorescence at 1270 nm, corresponding to the $O_2(^1\Delta_g) \rightarrow O_2(^3\Sigma_g^-)$ transition, after excitation of the nanofiber materials by a pulsed nanosecond laser. The time-resolved phosphorescence intensity plots (Figure 4, panel A) reveal the

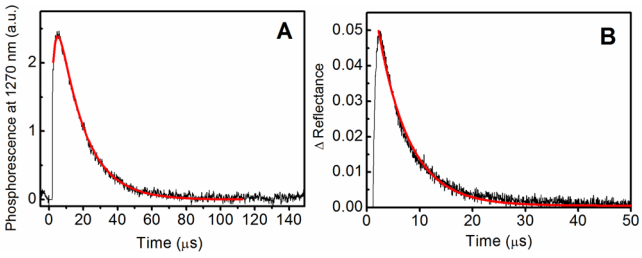

Figure 4. (A) Time-resolved phosphorescence of $O_2(^1\Delta_g)$ at 1270 nm and (B) time-resolved reflectance of the triplet state of **2-TPP** in an oxygen atmosphere. The red curves designate the fitting lines by the least-squares method (eq 3 and eq 1).

significant generation of $O_2(^1\Delta_g)$ in **2-TPP** by the quenching of the ^{3}TPP with $O_2(^3\Sigma_g^-)$ (Figure 4, panel B); similar signals were observed for all tested materials (before and after postprocessing modifications). The kinetics of $O_2(^1\Delta_g)$ can be described using a rise-and-decay model:[8]

$$[O_2(^1\Delta_g)] = A_{SO}\frac{\tau_\Delta}{\tau_T - \tau_\Delta}(\exp(-t/\tau_T) - \exp(-t/\tau_\Delta)) \quad (3)$$

where A_{SO} is a parameter that is proportional to the quantum yield of $O_2(^1\Delta_g)$ and τ_Δ is the lifetime of $O_2(^1\Delta_g)$.

Equations 1−3 provide good fits to the photophysical data (Figure 4). The values of τ_T, τ_Δ, and k_q calculated using fitting functions derived from eqs 1−3 are summarized in Table 1.

Oxygen Permeability and Diffusion Length of $O_2(^1\Delta_g)$. The oxygen-permeability values $P(O_2)$ (proportional to k_q) for all modified PS nanofiber materials (**2-TPP**, **3-TPP**, and **4-TPP**) were calculated from the slopes of the modified Stern−Volmer equation (eq 2) in the form of eq 4:[10]

$$1/\tau_T = 1/\tau_{T0} + 4.145\alpha 4\pi N_A \sigma P(O_2) p_{O2} \quad (4)$$

where α is the probability of quenching in the encounter complex, N_A is Avogadro's number, σ is the collision diameter of the ^{3}TPP−O_2 complex, and p_{O2} is the oxygen pressure. The values of α and σ were calculated from eq 4 using $P(O_2) = 1.9 \times 10^{-13}$ cm^3 cm/(cm^2 s Pa) for unmodified PS as the standard (Table 1).[10] Under the assumption that the oxygen solubility of $S(O_2) = 6.86 \times 10^{-7}$ cm^2 cm/(cm^3 Pa) remained unchanged in the bulk of the PS material,[10] the corresponding diffusion coefficient $D(O_2) = P(O_2)/S(O_2)$ could be determined.

The effective range of photogenerated $O_2(^1\Delta_g)$ inside the doped nanofibers was estimated using the diffusion equation. The mean radial diffusion length of $O_2(^1\Delta_g)$, $l_r = (6D(O_2)\tau_\Delta)^{1/2}$, was calculated from the values of τ_Δ that were obtained by measuring the decay time of the $O_2(^1\Delta_g)$ phosphorescence at 1270 nm and the calculated values of $D(O_2)$ for the individual PS nanofiber materials (Table 1). Evidently, the effective range of a photogenerated $O_2(^1\Delta_g)$ inside the material ($l_r \approx 44-47$ nm) was not significantly affected by any type of surface modification. For the typical $D(O_2)$ value in H_2O ($\sim 2 \times 10^{-5}$ cm^2 s^{-1}),[39] the maximum value for the l_r traveled by a photogenerated $O_2(^1\Delta_g)$ from the surface to a point in the aqueous surroundings of the nanofibers at which a substrate/target is located was calculated to be 205 nm for a typical value of $\tau_\Delta = 3.5$ μs in H_2O.[40] Thus, the diffusion length is sufficient only for the photo-oxidation of a substrate/target located in proximity to the surface.

Photo-Oxidation of External Substrates. The assumption that the wettability (inversely proportional to the ACA, Table 1) contributes to the photo-oxidation capability of the nanofiber materials was tested using a sensitive method based on the photo-oxidation of I^- to I_3^- in aqueous solutions.[31] The photoproduced concentration of I_3^- is directly proportional to the concentration of $O_2(^1\Delta_g)$. The relative photo-oxidation efficacy (PE) of the samples was calculated as the slope of the dependence of $A(I_3^-)/\sum I_0(1 - 10^{-A_i})$ on irradiation time, where $A(I_3^-)$ is the absorbance of the photoproduced I_3^- at 351 nm and $\sum I_0(1 - 10^{-A_i})$ is the sum of all absorbed light intensities at wavelengths λ_i (400−700 nm), which was compared with that of the **1-TPP** sample (Table 1, Figure 5). No photo-oxidation was observed in the dark upon irradiation in the absence of dissolved oxygen or upon the irradiation of the TPP-free nanofiber materials. No leakage of TPP into the aqueous solutions was detected. The PE values increased in D_2O because the effective lifetime of $O_2(^1\Delta_g)$ was higher by a factor of approximately 20 compared with that in H_2O.[41] The efficacy was nearly zero in the presence of NaN_3 (>0.01 mol L^{-1}), an effective quencher of $O_2(^1\Delta_g)$.[31]

The differences in photo-oxidation depended only on the intensity of absorbed light and the wettability of the surface because the nanofiber diameters, the photophysics of the photosensitizer, the permeability, and the diffusion coefficient of oxygen in the polymer matrix did not change (Table 1). The PE of the hydrophobic **1-TPP** sample was accelerated by all postprocessing modifications. For **2-TPP** (PE = 3.47) and **3-TPP** (PE = 3.50), the increase in photo-oxidation was nearly identical. The lower PE of **4-TPP** (PE = 1.44) can be primarily attributed to the filter effect of the light gray PDA coating, which reduced the transmittance of the pristine PS material in the TPP absorption region by 14.5−8% (Figure S9, Supporting

Table 1. Properties of Nanofiber PS Materials Doped with 1% TPP[a]

	PS nanofiber material			
	1-TPP	**2-TPP**	**3-TPP**	**4-TPP**
average nanofiber diameter (nm)	248 ± 29	253 ± 22	232 ± 20	268 ± 21
ACA (deg)	130	<5	<5	<5
τ_T (μs)	17.1	16.9	16.9	8.0
k_q (s^{-1} Pa^{-1})	1.9	1.8	1.7	1.7
τ_Δ (μs)	13.4	13.9	13.1	13.7
$P(O_2)$ (10^{13} cm^3 cm/(cm^2 s Pa))	1.9[b]	1.8	1.7	1.7
$D(O_2)$ (10^7 cm^2 s^{-1})	2.8	2.7	2.5	2.5
diffusion length (nm)	47	47	44	45
PE	1.0	3.47	3.50	1.44 (3.55[c])

[a] τ_T is the lifetime of the TPP triplet state (^{3}TPP) in an air atmosphere. k_q is the rate constant of the quenching of ^{3}TPP by oxygen. τ_Δ is the lifetime of the $O_2(^1\Delta_g)$ signal. $P(O_2)$ and $D(O_2)$ are the oxygen permeability and diffusion coefficients of the material, respectively, as calculated from the Stern–Volmer equation (eq 4), and PE is the relative photo-oxidation efficacy of I^- in an aqueous solution. [b] Standard used for the calculation of $P(O_2)$ (eq 4). [c] Corrected for the PDA filter effect.

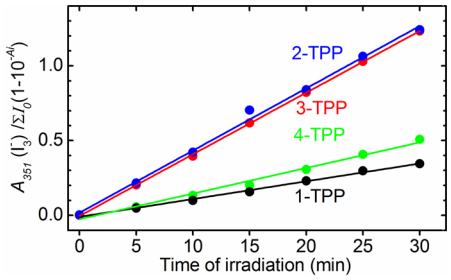

Figure 5. Time profiles of I_3^- absorbance at 351 nm related to the absorption of excitation light in 3 mL of an air-saturated, 0.05 M iodide detection solution containing a piece (2.5 cm^2) of **1-TPP** (black), **2-TPP** (blue), **3-TPP** (red), or **4-TPP** (green) under continuous irradiation at 25 °C. Irradiation source was a 500 W Xe lamp with a long-pass filter ($\lambda \geq 400$ nm).

Information). The PE of **4-TPP** can be approximately corrected for the filter effect using the expression $A(I_3^-)/\sum(T(\mathbf{4})_i/T(\mathbf{1})_i)I_0(1-10^{-A_i})$, where $T(\mathbf{4})_i/T(\mathbf{1})_i$ is the ratio of the individual transmittances of **4** and **1** at the corresponding λ_i, representing the decrease in the initial light intensity I_0. When the filter effect is considered, the value for **4-TPP** (PE = 3.55) attains a value similar to those of **2-TPP** and **3-TPP** within the estimated error of approximately 10%.

Antibacterial Activity. The role played by the wettability of the surfaces of the PS nanofiber materials in determining the surfaces' antibacterial activity was also tested using the procedure described in the Experimental Section. Figure 6 depicts an example of bacterial colonies on agar plates after inoculation with *E. coli* harvested from the surfaces (irradiated or stored in the dark) of **2** and **2-TPP** and incubation overnight. The agar plates that were inoculated with bacteria

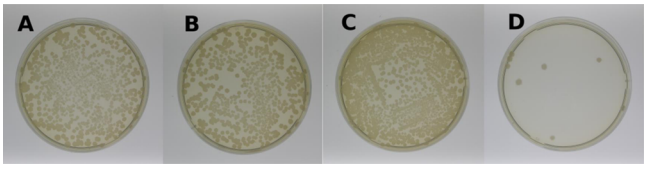

Figure 6. Colonies of *E. coli* on agar plates after inoculation with bacteria harvested from the surfaces of (A) **2** and (C) **2-TPP** stored in the dark and from the same materials after 20 min of irradiation and incubation overnight ((B) and (D), respectively). Irradiation was performed using a 400-W solar simulator equipped with a water filter.

from **2-TPP** stored in the dark and from irradiated **2** were used as negative controls. A very strong inhibition of bacterial growth was observed in the colonies from the **2-TPP** irradiated by visible light in contrast to both controls (**2-TPP** stored in the dark and irradiated **2**). This effect is attributed to the efficient photogeneration of antibacterial $O_2(^1\Delta_g)$.[8−11]

The **3-TPP** and **4-TPP** samples also exhibited high antibacterial efficiency compared with the hydrophobic **1-TPP** sample, whose antibacterial efficiency was low (Figure 7).

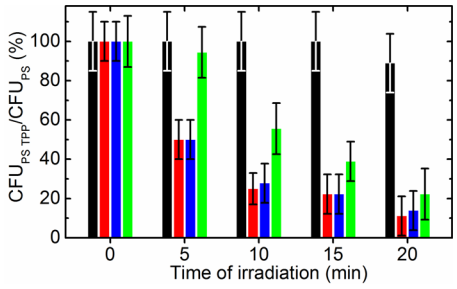

Figure 7. (Photo)antibacterial activity estimated as a proportion of the CFUs of *E. coli* observed on agar plates after inoculation with bacteria collected from the surfaces of samples with and without photosensitizer: **1-TPP**/**1** (black), **2-TPP**/**2** (red), **3-TPP**/**3** (blue), and **4-TPP**/**4** (green). The samples were irradiated by a 400 W solar simulator equipped with a water filter for 5, 10, 15, or 20 min and incubated overnight.

The antibacterial efficiencies of the samples represented in Figure 7 are consistent with their ability to oxidize external substrates (Table 1, Figure 5). Evidently, the surface composition has a significant effect on the surface wettability and, consequently, the bacterial adhesion. The increase in wettability achieved through postprocessing treatment increases the antibacterial efficiency on the surface because more bacterial pathogens lie within the cytotoxic diffusion range of $O_2(^1\Delta_g)$. It is known that PDA itself has a moderate antimicrobial effect, but this effect is correlated with the cells being coated with a layer of PDA controlling cell division and/or created barriers with reduced permeability to nutrients.[23] We did not observe any dark antibacterial effect on the surface of **4** or **4-TPP** (Table S1, Supporting Information). We also observed a much less efficient antibacterial effect for **4-TPP** on light due to filter effect of the PDA coating.

The experiment for the estimation of the antibacterial activity was designed to determine the activity as a proportion of the CFUs observed on the agar plates after inoculation with bacteria harvested from the surfaces of the samples with TPP (**1-TPP**, **2-TPP**, **3-TPP**, **4-TPP**) and from the corresponding samples without TPP (**1**, **2**, **3**, **4**) in the dark and under irradiation to eliminate the effect of the light itself and any differences in the intake of nutrients from the agar plates to the bacteria caused by the different functionalizations of the nanofiber surfaces. Although the antibacterial efficiencies of the samples with and without the photosensitizer can be directly compared under the same experimental conditions, the efficiencies of samples with different surfaces are difficult to compare with each other. In addition to the lack of homogeneity of the samples with a defined degree of derivatization and different intakes of nutrients, for **4** and **4-TPP**, we must consider the filter effect of the PDA coating. Nevertheless, the results clearly indicate that all hydrophilic modifications strongly increased the photoantibacterial activity toward *E. coli*. The differences arise with irradiation time (Figure 7, Table S1, Supporting Information). For example, 20 min of irradiation of **2-TPP** under simulated daylight caused a significant decrease in the number of CFUs (approximately 0−10% of the corresponding CFUs in the dark) in contrast to **1-TPP** (approximately 90% of the corresponding CFUs in the dark).

The low photoantibacterial efficiency on the surface of **1-TPP** is not as surprising if we calculate the portion of the volume of a water droplet of a bacterial suspension on the **1-TPP** surface that is accessible by $O_2(^1\Delta_g)$. For example, if we consider a 20 μL volume of inoculum as a model water droplet on the surface of **1-TPP** and a maximum diffusion length of 205 nm for $O_2(^1\Delta_g)$ in H_2O, the simple static mathematic model (Figure S10, Supporting Information) indicates that only approximately $^1/_{18000}$ of the total volume is accessible by $O_2(^1\Delta_g)$ in a certain time.

The photo-oxidation of the chemical substrate (I^-) and the photoantibacterial activity toward *E. coli* (an example of a biological target) in an aqueous environment clearly illustrate the key role of the surface wettability/hydrophilicity of $O_2(^1\Delta_g)$ photogenerating materials in both processes.

CONCLUSIONS

Here, we described the fabrication and properties of electrospun nanofiber materials with model TPP photosensitizer encapsulated in the hydrophobic PS nanofibers after three postelectrospinning modifications: sulfonation, oxygen plasma treatment, and the application of a thin PDA coating on the surface of the nanofiber material. All modifications strongly increased the wettability/hydrophilicity of the hydrophobic PS nanofibers without causing damage to the nanofibers, leakage of the photosensitizer, or any change in the spectral characteristics of TPP, the lifetime of the triplet state or singlet oxygen, or even the oxygen permeability of the polymer nanofibers. The increase in the surface wettability resulted in acceleration of the photo-oxidation of external substrates and an increase in the antibacterial activity of the nanofibers. The lower photo-oxidation and antibacterial efficiencies of nanofiber material with PDA coating in comparison with plasma treated and sulfonated materials are due to partial absorption of light by PDA.

These results reveal the crucial role played by surface hydrophilicity/wettability in ensuring the efficient photo-oxidation or photoinactivation of a chemical substrate or biological target at the surface of a material generating $O_2(^1\Delta_g)$ with a short diffusion length.

ASSOCIATED CONTENT

Supporting Information

Quantitative analysis of the (photo)antibacterial experiments, scheme of electrospinning device, SEM images of samples, photographs of samples with PDA coating, a demonstration of the self-stretching effect, ACA measurements of samples **1**−**4**, the diffuse reflectance and fluorescence spectra of the samples, the transmission spectra of the PS material, and a presentation of a model of a water droplet on the surface of PS material for the calculation of the volume accessible to $O_2(^1\Delta_g)$. This material is available free of charge via the Internet at http://pubs.acs.org.

AUTHOR INFORMATION

Corresponding Author

*E-mail: mosinger@natur.cuni.cz.

Notes

The authors declare no competing financial interest.

ACKNOWLEDGMENTS

This work was supported by the Czech Science Foundation (Grant 13-12496S). H.K. acknowledges the Czech Science Foundation (Grant P108/12/0910) for its support of the cold plasma experiments. The authors also thank Dr. Lukáš Plíštil for the preparation of the nanofiber materials via electrospinning.

REFERENCES

(1) Ma, Z.; Kotaki, M.; Ramakrishna, S. Surface Modified Nonwoven Polysulphone (PSU) Fiber Mesh by Electrospinning: A Novel Affinity Membrane. *J. Membr. Sci.* **2006**, *272*, 179−187.

(2) Hong, Y.; Li, Y.; Zhuang, X.; Chen, X.; Jing, X. Electrospinning of Multicomponent Ultrathin Fibrous Nonwovens for Semi-Occlusive Wound Dressings. *J. Biomed. Mater. Res., Part A* **2009**, *89A*, 345−354.

(3) Martins, A.; Chung, S.; Pedro, A. J.; Sousa, R. A.; Marques, A. P.; Reis, R. L.; Neves, N. M. Hierarchical Starch-Based Fibrous Scaffold for Bone Tissue Engineering Applications. *J. Tissue Eng. Regener. Med.* **2009**, *3*, 37−42.

(4) Yoon, K.; Hsiao, B. S.; Chu, B. Functional Nanofibers for Environmental Applications. *J. Mater. Chem.* **2008**, *18*, 5326−5334.

(5) Reneker, D. H.; Chun, I. Nanometer Diameter Fibres of Polymer, Produced by Electrospinning. *Nanotechnology* **1996**, *7*, 216−223.

(6) Greiner, A.; Wendorff, J. H. Electrospinning: A Fascinating Method for the Preparation of Ultrathin Fibres. *Angew. Chem., Int. Ed.* **2007**, *46*, 5670−5703.

(7) Henke, P.; Lang, K.; Kubát, P.; Sýkora, J.; Šlouf, M.; Mosinger, J. Polystyrene Nanofiber Materials Modified with an Externally Bound Porphyrin Photosensitizer. *ACS Appl. Mater. Interfaces* **2013**, *5*, 3776−3783.

(8) Mosinger, J.; Jirsák, O.; Kubát, P.; Lang, K.; Mosinger, B. Bactericidal Nanofabrics Based on Photoproduction of Singlet Oxygen. *J. Mater. Chem.* **2007**, *17*, 164−166.

(9) Mosinger, J.; Lang, K.; Kubát, P.; Sýkora, J.; Hof, M.; Plíštil, L.; Mosinger, B., Jr. Photofunctional Polyurethane Nanofabrics Doped by Zinc Tetraphenylporphyrin and Zinc Phthalocyanine Photosensitizers. *J. Fluoresc.* **2009**, *19*, 705−713.

(10) Jesenská, S.; Plíštil, L.; Kubát, P.; Lang, K.; Brožová, L.; Popelka, Š.; Szatmáry, L.; Mosinger, J. Antibacterial Nanofiber Materials Activated by Light. *J. Biomed. Mater. Res., Part A* **2011**, *99A*, 676−683.

(11) Arenbergerova, M.; Arenberger, P.; Bednar, M.; Kubat, P.; Mosinger, J. Light-Activated Nanofibre Textiles Exert Antibacterial

Effects in the Setting of Chronic Wound Healing. *Exp. Dermatol.* **2012**, *21*, 619−624.
(12) Lhotáková, Y.; Plíštil, L.; Morávková, A.; Kubát, P.; Lang, K.; Forstová, J.; Mosinger, J. Virucidal Nanofiber Textiles Based on Photosensitized Production of Singlet Oxygen. *PLoS One* **2012**, *7*, e49226.
(13) Mosinger, J.; Lang, K.; Plíštil, L.; Jesenská, S.; Hostomský, J.; Zelinger, Z.; Kubát, P. Fluorescent Polyurethane Nanofabrics: A Source of Singlet Oxygen and Oxygen Sensing. *Langmuir* **2010**, *26*, 10050−10056.
(14) Arai, T.; Tanaka, M.; Kawakami, H. Porphyrin-Containing Electrospun Nanofibers: Positional Control of Porphyrin Molecules in Nanofibers and Their Catalytic Application. *ACS Appl. Mater. Interfaces* **2012**, *4*, 5453−5457.
(15) Vesel, A.; Mozetic, M.; Hladnik, A.; Dolenc, J.; Zule, J.; Milosevic, S.; Krstulovic, N.; Klanjšek-Gunde, M.; Hauptmann, N. Modification of Ink-Jet Paper by Oxygen-Plasma Treatment. *J. Phys. D: Appl. Phys.* **2007**, *40*, 3689−3696.
(16) Médard, N.; Soutif, J.; Poncin-Epaillard, F. CO_2, H_2O, and CO_2/H_2O Plasma Chemistry for Polyethylene Surface Modification. *Langmuir* **2002**, *18*, 2246−2253.
(17) Sowe, M.; Novák, I.; Vesel, A.; Junkar, I.; Lehocký, M.; Sáha, P.; Chodák, I. Analysis and Characterization of Printed Plasma-Treated Polyvinyl Chloride. *Int. J. Polym. Anal. Charact.* **2009**, *14*, 641−651.
(18) Junkar, I.; Cvelbar, U.; Vesel, A.; Hauptman, N.; Mozetič, M. The Role of Crystallinity on Polymer Interaction with Oxygen Plasma. *Plasma Processes Polym.* **2009**, *6*, 667−675.
(19) Vesel, A. Modification of Polystyrene with a Highly Reactive Cold Oxygen Plasma. *Surf. Coat. Technol.* **2010**, *205*, 490−497.
(20) Vesel, A.; Junkar, I.; Cvelbar, U.; Kovac, J.; Mozetic, M. Surface Modification of Polyester by Oxygen- and Nitrogen-Plasma Treatment. *Surf. Interface Anal.* **2008**, *40*, 1444−1453.
(21) Lee, H.; Dellatore, S. M.; Miller, W. M.; Messersmith, P. B. Mussel-Inspired Surface Chemistry for Multifunctional Coatings. *Science* **2007**, *318*, 426−430.
(22) Ye, Q.; Zhou, F.; Liu, W. Bioinspired Catecholic Chemistry for Surface Modification. *Chem. Soc. Rev.* **2011**, *40*, 4244−4258.
(23) Iqbal, Z.; Lai, E. P. C.; Avis, T. J. Antimicrobial Effect of Polydopamine Coating on *Escherichia coli*. *J. Mater. Chem.* **2012**, *22*, 21608−21612.
(24) Liebscher, J.; Mrówczyński, R.; Scheidt, H. A.; Filip, C.; Hădade, N. D.; Turcu, R.; Bende, A.; Beck, S. Structure of Polydopamine: A Never-Ending Story? *Langmuir* **2013**, *29*, 10539−10548.
(25) Dreyer, D. R.; Miller, D. J.; Freeman, B. D.; Paul, D. R.; Bielawski, C. W. Elucidating the Structure of Poly(dopamine). *Langmuir* **2012**, *28*, 6428−6435.
(26) Vasilev, K.; Griesser, S. S.; Griesser, H. J. Antibacterial Surfaces and Coatings Produced by Plasma Techniques. *Plasma Processes Polym.* **2011**, *8*, 1010−1023.
(27) Phua, S. L.; Yang, L.; Toh, C. L.; Guoqiang, D.; Lau, S. K.; Dasari, A.; Lu, X. Simultaneous Enhancements of UV Resistance and Mechanical Properties of Polypropylene by Incorporation of Dopamine-Modified Clay. *ACS Appl. Mater. Interfaces* **2013**, *5*, 1302−1309.
(28) Forward, K. M.; Rutledge, G. C. Free Surface Electrospinning from a Wire Electrode. *Chem. Eng. J.* **2012**, *183*, 492−503.
(29) An, H.; Shin, C.; Chase, G. G. Ion Exchanger Using Electrospun Polystyrene Nanofibers. *J. Membr. Sci.* **2006**, *283*, 84−87.
(30) Yang, H.; Lan, Y.; Zhu, W.; Li, W.; Xu, D.; Cui, J.; Shen, D.; Li, G. Polydopamine-Coated Nanofibrous Mats as a Versatile Platform for Producing Porous Functional Membranes. *J. Mater. Chem.* **2012**, *22*, 16994−17001.
(31) Mosinger, J.; Mička, Z. Quantum Yields of Singlet Oxygen of Metal Complexes of meso-Tetrakis(sulphonatophenyl)porphine. *J. Photochem. Photobiol., A* **1997**, *107*, 77−82.
(32) Socrates, G. *Infrared and Raman Characteristic Group Frequencies: Tables and Charts*, 3rd ed; John Wiley & Sons: New York, 2004.
(33) Lee, M. W.; An, S.; Latthe, S. S.; Lee, C.; Hong, S.; Yoon, S. S. Electrospun Polystyrene Nanofiber Membrane with Superhydrophobicity and Superoleophilicity for Selective Separation of Water and Low Viscous Oil. *ACS Appl. Mater. Interfaces* **2013**, *5*, 10597−10604.
(34) Lim, H. S.; Park, S. H.; Koo, S. H.; Kwark, Y.-J.; Thomas, E. L.; Jeong, Y.; Cho, J. H. Superamphiphilic Janus Fabric. *Langmuir* **2010**, *26*, 19159−19162.
(35) Dreyer, D. R.; Miller, D. J.; Freeman, B. D.; Paul, D. R.; Bielawski, C. W. Perspectives on Poly(dopamine). *Chem. Sci.* **2013**, *4*, 3796−3802.
(36) Chai, J.; Lu, F.; Li, B.; Kwok, D. Y. Wettability Interpretation of Oxygen Plasma Modified Poly(methyl methacrylate). *Langmuir* **2004**, *20*, 10919−10927.
(37) Kubat, P.; Lang, K.; Prochazkova, K.; Anzenbacher, P. Self-Aggregates of Cationic meso-Tetratolylporphyrins in Aqueous Solutions. *Langmuir* **2003**, *19*, 422−428.
(38) Procházková, K.; Zelinger, Z.; Lang, K.; Kubát, R. Meso-Tetratolylporphyrins Substituted by Pyridinium Groups: Aggregation, Photophysical Properties and Complexation with DNA. *J. Phys. Org. Chem.* **2004**, *17*, 890−897.
(39) Tsushima, M.; Tokuda, K.; Ohsaka, T. Use of Hydrodynamic Chronocoulometry for Simultaneous Determination of Diffusion Coefficients and Concentrations of Dioxygen in Various Media. *Anal. Chem.* **1994**, *66*, 4551−4556.
(40) Poulsen, T. D.; Ogilby, P. R.; Mikkelsen, K. V. Solvent Effects on the $O_2(a^1\Delta_g)-O_2(X^3\Sigma_g^-)$ Radiative Transition: Comments Regarding Charge-Transfer Interactions. *J. Phys. Chem. A* **1998**, *102*, 9829−9832.
(41) Wilkinson, F.; Helman, W. P.; Ross, A. B. Rate Constant for the Decay and Reactions of the Lowest Electronically Excited Singlet State of Molecular Oxygen in Solution—An Expanded and Revised Compilation. *J. Phys. Chem. Ref. Data* **1995**, *24*, 663−1021.